Int. J. Electrochem. Sci., 14 **(2019)** 238 – 249, doi: 10.20964/2019.01.10

International Journal of
ELECTROCHEMICAL
SCIENCE
www.electrochemsci.org

Electrode materials based on Micro-emulsion Polymerized Polyaniline and Their Capacitive Property

Lijun Ren[*], *Gaini Zhang, Huiqin Li, Dengwei Hu, Shumei Dou*

College of Chemistry and Chemical Engineering, Engineering Research Center of Advanced Ferroelectric Functional Materials, Key Laboratory of Phytochemistry, Baoji University of Arts and Sciences, Baoji, 721013, P. R. China
[*]E-mail: renlijun.wind@163.com

Received: 14 September 2018 / *Accepted:* 22 October 2018 / *Published:* 30 November 2018

The conductive polyaniline (PANI) electrode materials with different morphologies were prepared by micro-emulsion polymerization with dodecylbenzene sulfonic acid (DBSA) as the dopant and surfactant, and ammonium persulfate (APS) as the oxidant. The concentration of DBSA was crucial in tailoring the morphology of PANI. Electrochemical tests showed that the capacitive properties of the electrode materials were influenced markedly by their morphologies and conductivities. At low DBSA concentration, the obtained PANI nanoribbon (PANI-1) electrode processed high specific capacitance (573 F g^{-1} at a current density of 0.2 A g^{-1}) and excellent rate performance (78% capacitance retention from 0.2 to 10 A g^{-1}) but showed poor cycling stability. Furthermore, the specific capacitance and rate performance of the resultant PANI electrodes were decreased with increase in the concentration of DBSA. At high DBSA concentration, the specific capacitance and rate performance of the obtained PANI nanoparticle (PANI-4) electrode decreased to 205 F g^{-1} (0.2 A g^{-1}) and 63% (from 0.2 to 10 A g^{-1}), respectively. Nevertheless, it possessed superior cycling stability with just 8% capacitance loss after 2000 charging/discharging cycles.

Keywords: Polyaniline; Dodecylbenzene sulfonic acid; Micro-emulsion polymerization; Electrode material; Supercapacitor

1. INTRODUCTION

Supercapacitors (SCs) are one of the most promising energy sources for back-up power devices, cell phones, and hybrid electric vehicles, due to their superior power delivery, fast charging/discharging rate, and long cycle life [1–3]. As a critical component in SCs, the electrode materials play an important role in determining the overall performance of SCs [4]. The most striking characteristic is that the capacitive properties of the electrode materials depend on their sizes and shapes when the dimensions

are scaled down to the nano-level [5]. Therefore, it is necessary to develop reliable preparation methods that can precisely tailor the nanostructure of electrode materials. Many researches have been focused on the design and preparation of various kinds of electrode materials [6, 7]. However, compared to inorganic nanomaterials, it is intrinsically difficult to control the morphology of organic polymer nanomaterials whose dimensional stabilities drop dramatically at the nanoscale level [8].

Polyaniline (PANI) has become one of the attractive cathode candidate materials for SCs due to its high electrical conductivity, ease of synthesis, low cost, and reversibility between redox states through doping/dedoping processes [9]. It has been proven that the nanostructure of PANI can remarkably affect its capacitive property [10]. In recent years, a large number of nanostructured PANI (nano-fibers/nanorods/nanowires/nanotubes) were prepared by a variety of approaches including template preparation method, electrochemical deposition, interfacial polymerization, and micro-emulsion polymerization, which improved their electrochemical properties [5, 11-13]. Among these, micro-emulsion polymerization is known to be one of the most effective methods among various preparation methods [14, 15]. Surfactants are usually appear in the micro-emulsion polymerization system, which are amphiphilic molecules that are known to lower the surface tension of a liquid and to form micelles. Because of their nature, when incorporated into the micro-emulsion polymerization system, they effectively control the growth of particles [16].

Up to now, very less attention has been paid attention to the assembly behaviors of the PANI nanomaterials and the resulting capacitive properties. Here we report preparation of PANI electrode materials with different morphologies by micro-emulsion polymerization with dodecylbenzene sulfonic acid (DBSA) as the dopant and surfactant, and ammonium persulfate (APS) as the oxidant at 20 °C. In the micro-emulsion polymerization experiment system, where aniline monomers in the cationic form formed complexation with DBSA micelles, which in turn determine the PANI morphology grown. The morphologies and sizes of PANI nanostructures could be tailored by the concentration of DBSA surfactant. The remarkable capacitance characteristics of the PANI nanostructures could be attributed to their morphologies and conductivities. To verify it, the analyses of molecular structures, aggregation processes and capacitive properties have been studied in detail.

2. EXPERIMENTAL SECTION

2.1 Materials preparation

Aniline (An, analytical grade) was distilled until color-less under reduced pressure before use. Other chemicals (analytical grade) were used as received without further treatment.

Preparation of PANI electrode materials with different morphologies: The PANI electrode materials were prepared by a simple micro-emulsion polymerization of aniline monomers using DBSA as the surfactant and APS as the oxidizer. Solution A: Firstly, different mass of DBSA (50, 80, 100, and 200 mg) were dissolved in 0.1 M HCl (35 mL) aqueous solution, then 150 μL aniline was added into the above solution and stirred for 1 h at 20 °C. Solution B: 380 mg APS was dissolved into 0.1 M HCl (10 mL) aqueous solution. Finally, solution B was added into solution A and stirred continually for 3 h

at 20 °C. The obtained precipitates were followed by washing with ultrapure water and ethanol, and dried in a vacuum at 60 °C for 10 h, the PANI electrode materials PANI-1, PANI-2, PANI-3, PANI-4 were finally obtained when the different concentrations of DBSA (0.0034, 0.0054, 0.0068, and 0.0136 mol/L) were used in the reaction.

2.2 Characterization

A SU8020 field-emission scanning electron microscopy (FESEM) was used to observe the morphology of the obtained materials. Infrared spectra (FTIR) were obtained by KBr method on a Fourier Transform Infrared Spectrometer EQUINX55. Raman spectra were measured on a Renishaw inVia Raman microscope with an excitation wavelength of 785 nm. The electrochemical properties of the electrode materials were studied on a CHI 660E (Chenhua, Shanghai) electrochemical workstation.

2.3 Electrochemical measurement

The electrochemical properties of the obtained electrode materials were studied by cyclic voltammetry (CV), galvanostatic charge-discharge (GCD) and electrochemical impedance spectroscopy (EIS) in a three electrode system. Electrodes were prepared by mixing electro-active materials, acetylene black and PTFE (polytetrafluoroethylene) in a mass ratio of 85:10:5 to form homogenous slurry. Then the slurry was spread onto the stainless steel cloth (Mesh sizes 500) (1 cm^2) and dried at 60 °C for 10 h. After drying, the coated mesh was pressed to form working electrodes. The loading mass of the active material was about ~3 mg. The electrochemical tests were performed using 1.0 H_2SO_4 as electrolyte. The specific capacitance of the electrode was calculated from the galvanostatic discharge process according to the following equation: $Cs = I \times t/(V \times m)$, where I is the discharge current (A), t is the discharge time (s), V is the voltage change (V) excluding the IR drop during the discharge process, and m is the total mass of the active material for both electrodes (g). The electrochemical impedance spectroscopy (EIS) was performed with an amplitude of 5 mV at a frequency range of 0.01 to 100 kHz.

3. RESULTS AND DISCUSSION

Micro-emulsion polymerization method is a simple and reliable process for preparation of high quality nanostructured PANI materials with tailoring capacitive properties.

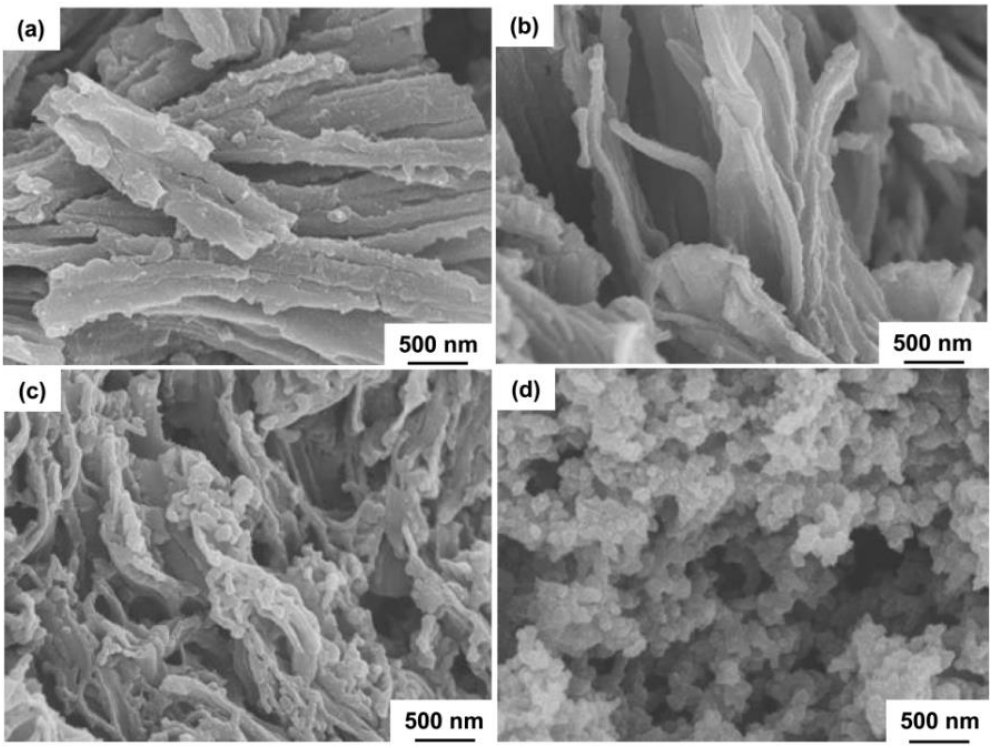

Figure 1. FESEM images of PANI electrode materials prepared using different concentrations of DBSA: (a) PANI-1 ([DBSA] = 0.0034 mol L^{-1}), (b) PANI-2 ([DBSA] = 0.0054 mol L^{-1}), (c) PANI-3 ([DBSA] = 0.0068 mol L^{-1}), and (d) PANI-4 ([DBSA] = 0.0136 mol L^{-1})

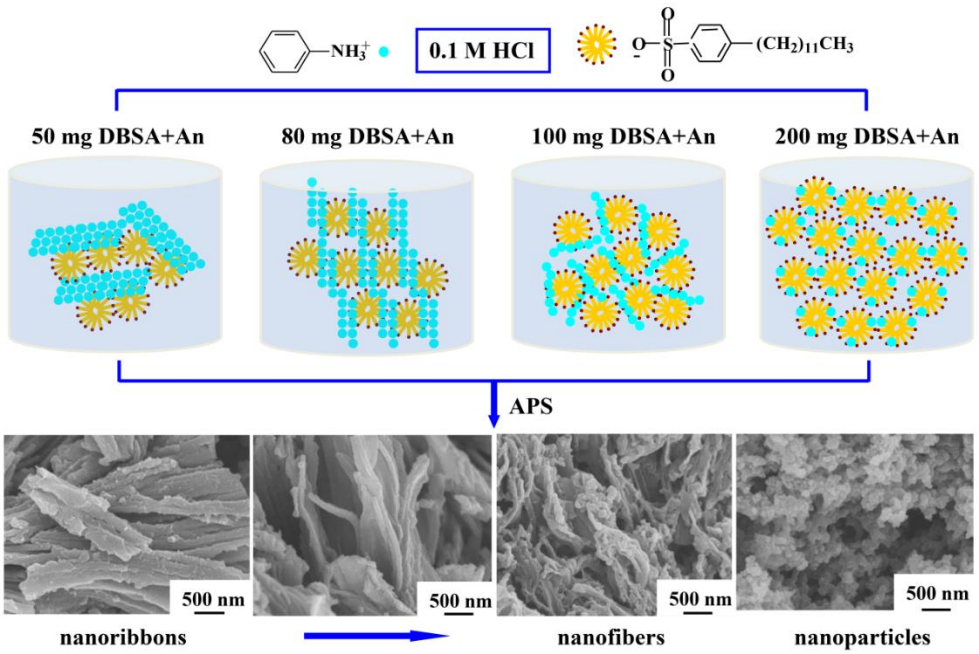

Figure 2. Schematic illustration of the possible complexation morphologies between DBSA and aniline cationic to prepare PANI electrode materials

In this work, PANI electrode materials were prepared by micelle-induced self-assembly of aniline monomers, followed by in situ polymerization of PANI. Assisted by HCl, the anilinium cations

formed complexation with micelles of dodecylbenzene sulfonate anions. As a result, PANI with different morphologies were obtained. As shown in Figure S1, a rock-like structure was readily obtained without using of any structure directing DBSA agent.

However, in the presence of DBSA, the morphologies of the resulting PANI materials could be tuned instead to nanoribbons, nanofibers or nanoparticles, which depending on the concentration of DBSA. Figure 1 exhibits the FESEM images of PANI nanostructures prepared using different concentrations of DBSA. It could be seen that the presence of the surfactant impacts the nanostructure of the final material significantly.

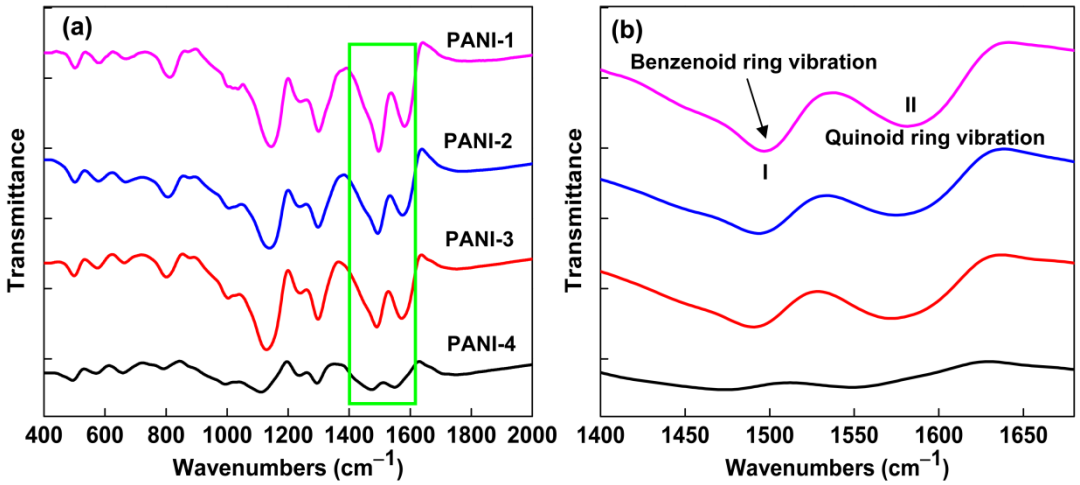

Figure 3. (a) FTIR spectra of PANI electrode materials and (b) the expanded view of 1400~1680 cm^{-1} region

When the concentration of DBSA was 0.0034 mol L^{-1}, PANI nanoribbons with diameters of ~500 nm and lengths of ~3 μm were formed. When the concentration of DBSA was increased to 0.0054 mol L^{-1}, a few of PANI nanofibers appeared. When the concentration of DBSA was twice of the original concentration, PANI nanofibers are formed with a diameter of ~80 nm. With sufficiently high concentration of DBSA (0.0136 mol L^{-1}), PANI nanoparticles with a diameter of ~120 nm are found. One of the key factors controlling the electrochemical behavior of conducting polymers is morphology, and modification of PANI morphology can lead to better SC performance [17].

The morphological evolution of PANI nanostructures from nanoribbons to nanofibers and nanoparticles was studied by FESEM. On the basis of the above observation, a mechanism for the growth of PANI with different morphologies was proposed (Figure 2): (i) The DBSA anionic surfactant formed micelles, and aniline formed the cationic form after aniline monomers were introduced into the reaction system. (ii) Aniline cationic complexed with DBSA anions via Coulumbic attractions between $-NH_3^+$ and $-SO_3^-$ and the mixed micelles acquired different shapes depending on the concentration of DBSA anions, essentially to minimize the total energy of the system. Thus the morphologies and sizes of PANI nanostructures could be tailored by the concentration of DBSA surfactant after the addition of APS oxidant [15].

Surfactants interfere with particle growth, which in turn influence the structures and properties of PANI electrode materials [16]. Their ability to induce structural changes could be useful to control the capacitive properties of the resultant PANI electrode materials. FTIR and Raman studies were carried out in order to characterize the molecular structures of PANI electrode materials. The FTIR spectra of the resultant PANI electrode materials prepared using different concentrations of DBSA surfactant are shown in Figure 3. It could be seen that characteristic bands for each PANI sample were almost the same. The spectra exhibited the characteristic bands at around 1575 and 1490 cm^{-1}, corresponding to the C=C stretching vibrations of quinoid and benzenoid rings, respectively [18-20]. The other bands at 1295, 1130, and 805 cm^{-1} could be assigned to the C−N stretching vibration, the C−H in plane bending vibration and the C−H out of plane bending vibration, respectively [21]. These characteristic bands indicated that all the four PANI electrode materials were identical to the emeraldine salt form. Particularly, the bands at 1010 and 505 cm^{-1} could be assigned to the absorption of $–SO_3H$ group of doped DBSA [15].

Table 1. The intensity ratios of I_{II}/I_I in FTIR spectra of the PANI electrode materials

PANI samples	PANI-1	PANI-2	PANI-3	PANI-4
I_{II}/I_I	0.77	0.79	0.88	0.92

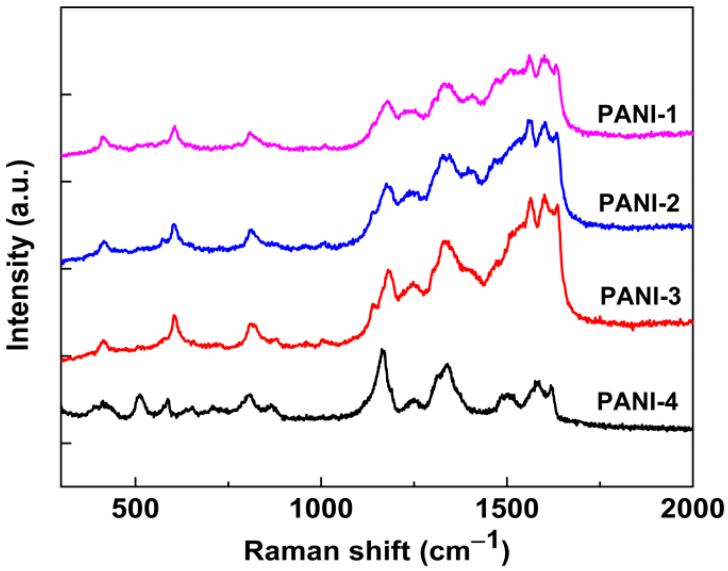

Figure 4. Raman spectra of PANI electrode materials

Additionally, the intensities of the absorption peaks at 1575 and 1490 cm^{-1} showed significant changes with varying DBSA concentration (Figure 3b), the intensity ratios I_{II}/I_I of the PANI materials increased with increase in DBSA concentration from 0.77 to 0.92. All the characteristic bands were shifted to lower wavenumbers (red shift) from PANI-1 to PANI-4, which indicated that the conjugated effect of the PANI long chain are strengthened and the conductivity becomes better from PANI-1 to PANI-4 [18]. Raman spectra of the prepared PANI electrode materials are shown in Figure 4. The C–C stretching of benzenoid ring and C–C stretching in the range of 1561~1635 cm^{-1}, the vibrations of the

semiquinone radicals at 1334 cm^{-1}, C–H bending of quinoid or benzenoid ring at 1170 cm^{-1} were observed for all samples, indicating the structure of PANI is in doping state [19, 22, 23].

Table 2. Comparison of capacitive properties with reported values

PANI electrode materials	Specific capacitance	Capacitance retention	Cycling stability	References
nanofibers/nanosflowers /nanorods/nanotubes	521/543/638/661 F g^{-1} (1 A g^{-1})	50/70/75/88% (1~10 A g^{-1})	58/59/58/63% (1000 C)	[5]
nanospheres/nanorods /nanofibers	71/133/192 F g^{-1} (0.1 A g^{-1})	nearly 0% (0.1~10 A g^{-1})	——	[8]
nanofibers/nanoparticles /helixes	159/163/190 F g^{-1} (0.5 A g^{-1})	66/39/72% (0.5~10 A g^{-1})	72/66/79% (2000 C)	[10]
nanorods	279 F g^{-1} (0.5 A g^{-1})	50% (0.5~50 A g^{-1})	45% (2200 C)	[26]
nanoribbons/nanofibers /nanoparticles	573/405/205 F g^{-1} (0.2 A g^{-1})	78/69/63% (0.2~10 A g^{-1})	52/80/92% (2000 C)	This work

The capacitive properties of as prepared materials were fully investigated by CV, GCD, EIS and cycle life measurement in 1 M H_2SO_4. In Figure 5a, the CV profiles of PANI electrodes distinctly showed two pairs of redox peaks, suggesting typical pseudocapacitive characteristics of the PANI electrode [24]. The first pair of redox peaks could be ascribed to the transformation between the leucoemeraldine base (LB) and emeraldine salt (ES) states of PANI, while the second pair of redox peaks was due to the transformation between emeraldine salt (ES) and pernigraniline base (PB) states [25]. The integration areas of CV profiles increased with decrease in DBSA concentration. This clearly indicated that the integration area of CV profile for PANI-1 electrode was larger than those of other three PANI electrodes, indicating a desirable capacitance due to PANI nanoribbon electrode could offer more active sites for redox charge transfer.The same trend could be seen in the comparison of GCD curves for various samples at a current density of 0.2 A g^{-1} (Figure 5b). As expected, the PANI-1 electrode had a longer charging/discharging time than the other three electrodes owing to its high capacitance. All the electrodes made from the four kinds of PANI materials show typical symmetric curves, and the minor distorted GCD curves could also be observed, which was associated with the redox characteristics of PANI [24].

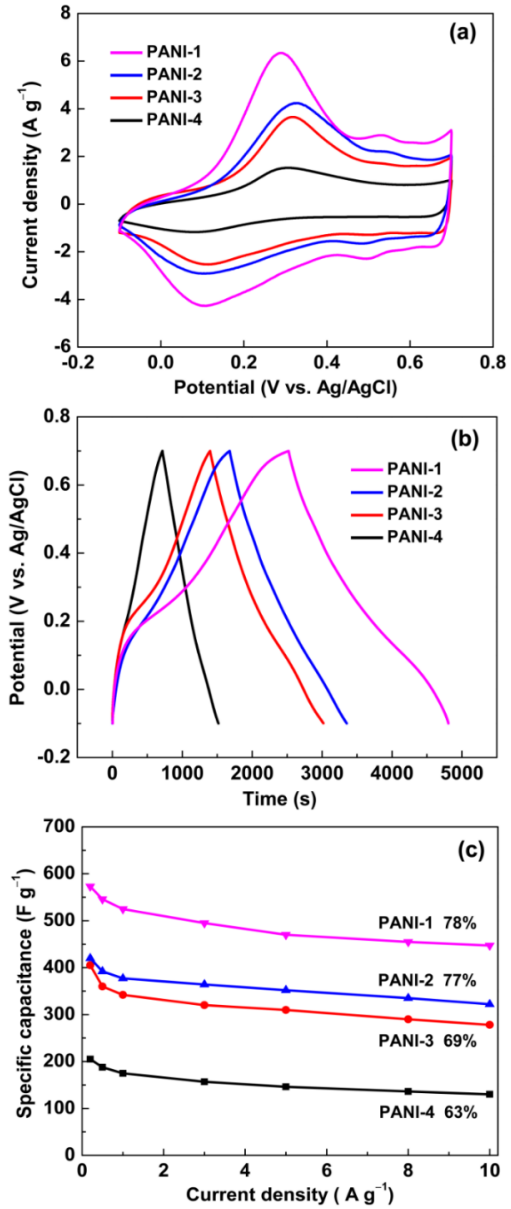

Figure 5. Capacitive properties of PANI electrodes in 1 M H_2SO_4 electrolyte: (a) CV profiles at 5 mV s^{-1}, (b) GCD curves at 0.2 A g^{-1}, and (c) capacitance variation from 0.2 to 10 A g^{-1}

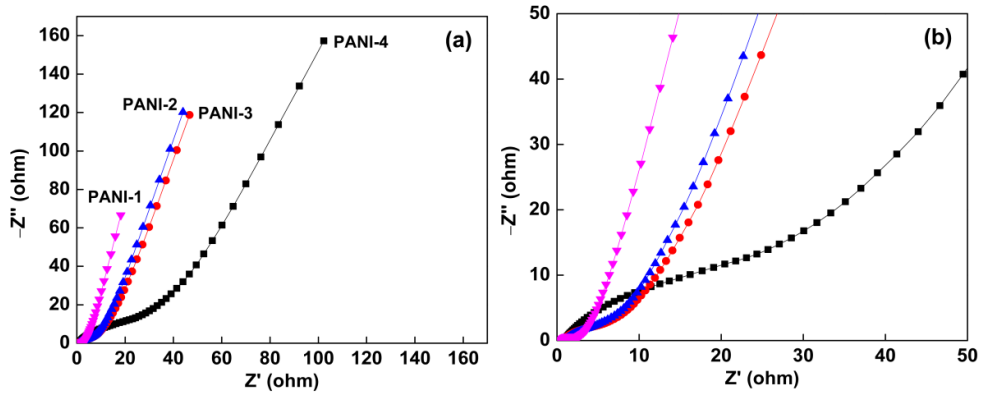

Figure 6. (a) Nyquist plots measured at frequency range from 100 kHz to 0.01 Hz and (b) the close-up view of the high-frequency region of Nyquist plots

With the increase of DBSA concentration, the discharging times of the PANI electrodes became shorter, which indicated that an increase in surfactant concentration resulted in poor redox reactions. The differences in the capacitance performance of the four electrodes could be assigned to the diverse morphologies of PANI nanostructure. The rate performance of the PANI electrodes were further investigated at different current densities from 0.2 to 10 A g^{-1} (Figure 5c). It was evident that the specific capacitance gradually decreased with increase in current density. The capacitive retentions of four PANI electrodes from 0.2 to 10 A g^{-1} were 78, 77, 69, and 63% for PANI-1, PANI-2, PANI-3, and PANI-4, respectively. This indicated that the electrodes with lower DBSA concentration had excellent rate performance. Moreover, the specific capacitance of PANI-1 electrode was always higher than those of other three electrodes. The better rate performance for PANI-1 electrode could probably be ascribed to its highly delocalized conjugated structure with high conductivity, which improved the rate of ion transportation. As shown in table 2, the specific capacitance and rate performance of PANI-1 were comparable to the reported PANI electrode materials [5, 8, 10, 26].

EIS is a technique which complements GCD measurements and provides more information on the electrochemical frequency behavior of the system. Impedance measurements can also be used to study the redox reaction resistance and equivalent series resistance [27]. In this study, the EIS data were analyzed using Nyquist plots in this study, and the Nyquist plots of four PANI electrodes with different morphologies are shown in Figure 6. They showed a semicircular pattern in the high-frequency region followed by a straight line in the low-frequency region for each electrode. The semicircles became larger and the straight lines became more and more close to 45° from PANI-1 to PANI-4. The largest semicircles was observed for PANI-4 electrode is indicative of high interfacial charge-transfer resistance, which could be attributed to its poor electrical conductivity [28]. The 45° sloped portion of PANI-4 electrode was the Warburg resistance resulting from the frequency dependence of ion diffusion/transport in the electrolyte, its larger Warburg region indicates greater variations in ion diffusion path lengths and increased obstruction of ion movement [27]. More interestingly, the semicircle was smallest for PANI-1 electrode, suggesting that its interfacial charge transfer resistance was significantly low, which due to the high conductivity. Except for the low electrical resistance, PANI-1 electrode also showed a short and equal diffusion path length of the ions in the electrolyte, which could be seen from the neglectable Warburg region on the Nyquist plots. Moreover, PANI-1 electrode had more vertical line than other three PANI electrodes at low frequency, revealing an ideally capacitive behavior due to the fast and reversible faradic reaction on PANI nanoribbon electrode [29]. This may be illuminated by the unique morphology, thus the ions of electrolyte do not penetrate into the particulate and access only the surface of PANI nanoribbons.

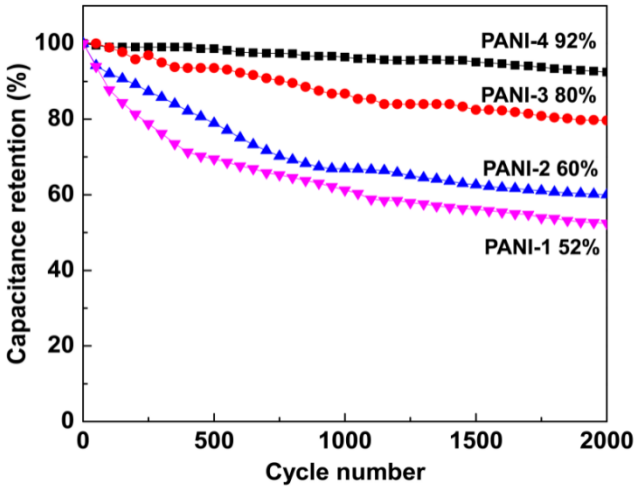

Figure 7. Cycling performance of PANI electrodes at 5 A g^{-1} for 2000 cycles in 1 M H_2SO_4 electrolyte

Another important parameter of electrode materials for SCs is cycling performance. As exhibited in Figure 7, after 2000 consecutive cycles at a current density of 5 A g^{-1}, the specific capacitances of the PANI-1, PANI-2, PANI-3, and PANI-4 electrodes retained about 52, 60, 80, and 92% of their original capacitances, respectively. It was obvious that the better long-term electrochemical stability was achieved at higher DBSA concentration. In comparison with other three PANI electrodes, PANI-4 electrode showed relatively better cycling performance. This capacitance retention was also better than those of earlier reported PANI electrode materials. For example, Zhou's group reported PANI helixe, nanofiber, and nanoparticle electrodes had 79, 72 and 66% of the original values retain after 2000 cycles, respectively [10], and the PANI nanofiber electrode reported by Du's group retained only 45% value of initial specific capacitance after 2200 cycles [26]. The small nanoparticles of PANI-4 electrode could restrict the volume changes during insertation/deinsertation processes, which further improved the cycling stability [30]. The above results indicated that the conductivities and morphological differences of DBSA doped PANI electrode materials have great influence on their capacitance behavior, ie. specific capacitance, rate performance and cycling stability.

4. CONCLUSION

The successfully preparation of PANI nanoribbons, nanofibers and nanoparticles via micro-emulsion polymerization using DBSA as dopant and surfactant enabled the investigation of the influence of nanostructure on the capacitance properties of PANI electrodes. The morphologies and sizes of PANI were tailored by varying the concentration of DBSA surfactant. The PANI nanoribbon electrode exhibited better specific capacitance and rate performance than those of other PANI electrodes because of its higher conductivity. However, the PANI nanoparticle electrode possessed superior cycling stability with 92% capacitance retention after 2000 consecutive charging/discharging cycles which contributed to the restriction of the electrode volume change. This study provided a new approach to control the nanostructure and capacitive properties of PANI electrode materials. It is expected that the above findings may provide a new insight into the tailoring of polymer nanostructures as well as an essential understanding of the parameters determining the capacitive properties of electrode materials.

SUPPORTING MATERIAL:

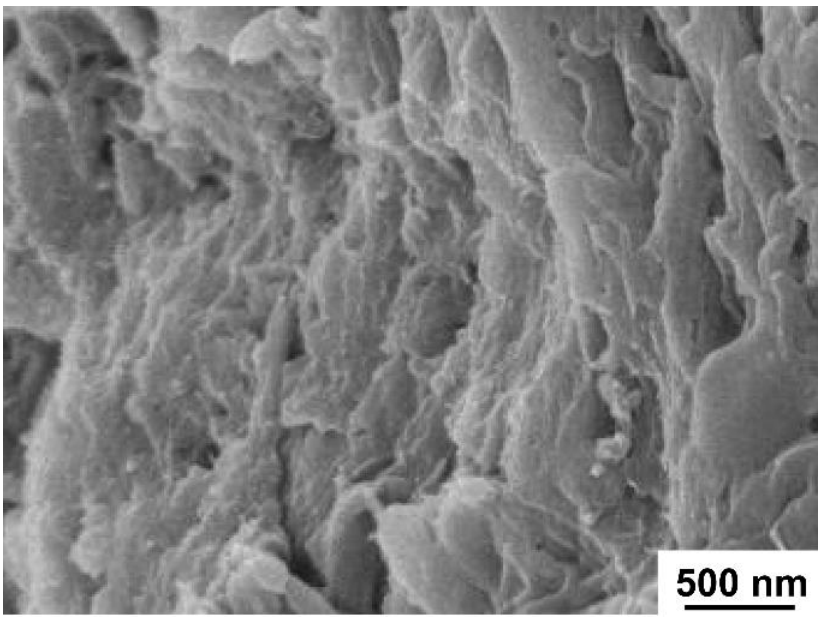

Figure S1. FESEM image of PANI prepared without DBSA surfactant

ACKNOWLEDGEMENT
This work was supported by the National Natural Science Foundation of China (51702006), the Natural Science Foundation Research Project of Shaanxi Province (2018JQ2065 and 2018JQ2068), the Scientific Research Project of Shaanxi Province Office of Education (16JK1040), the Science and Technology Project of Baoji (2017JH2-04) and the Doctoral Scientific Research Starting Foundation of Baoji University of Arts and Science (ZK2017031 and ZK2017028).

References

1. K. S. Kumar, N. Choudhary, Y. Jung, J. Thomas, *ACS Energy Lett.,* 3 (2018) 482−495.
2. N. Choudhary, C. Li, J. Moore, N. Nagaiah, L. Zhai, Y. Jung, J. Thomas, *Adv. Mater.,* 29 (2017) 1605336−1605345.
3. H. Sun, Y. Zhang, J. Zhang, X. M. Sun, H. S. Peng, *Nat. Rev. Mater.,* 2 (2017) 17023−17034.
4. J. E. Elshof, H. Yuan, P. G. Rodriguez, *Adv. Energy Mater.,* 6 (2016) 1600355−1600388.
5. L. J. Ren, G. N. Zhang, J. F. Wang, L. P. Kang, Z. B. Lei, Z. W. Liu, Z. T. Liu, Z. P. Hao, Z. H. Liu, *Electrochim. Acta,* 145 (2014) 99−108.
6. W. Liu, M. S. Song, B. Kong, Y. Cui, *Adv. Mater.,* 29 (2017) 1603436−1603469.
7. B. M. Sánchez and Y. Gogotsi, *Adv. Mater.,* 28 (2016) 6104−6135.
8. H. W. Park, T. Kim, J. Huh, M. Kang, J. E. Lee, H. Yoon, *ACS Nano,* 6 (2012) 7624−7633.
9. W. W. Li, F. X. Gao, X. Q. Wang, N. Zhang, M. M. Ma, *Angew. Chem. Int. Ed.,* 55 (2016) 9196 – 9201.
10. C. Li, L. Yang, Y. Meng, X. J. Hu, Z. X. Wei, P. Chen, *RSC Adv.,* 3 (2013) 21315−21319.
11. H. D. Tran, J. M. D'Arcy, Y. Wang, P. J. Beltramo, V. A. Strong, R. B. Kane, *J. Mater. Chem.* 21 (2011) 3534−3550.
12. D. Li, J. Huang, R. B. Kaner, *Accounts Chem. Res.,* 42 (2009) 135−145.
13. Y. Z. Long, M. M. Li, C. Z. Gu, M. X. Wan, J. L. Duvail, Z. W. Liu, Z. Y. Fan, *Prog. Polym. Sci.* 36 (2011) 1415–1442.

14. Li Wei, Q. Chen, Y. J. Gu, *J. Alloy. Com.*, 501 (2010) 313–316.
15. D. T. Ge, L. L. Yang, A. Honglawan, J. Li, S. Yang, *Chem. Mater.*, 26 (2014) 1678−1685.
16. J. P. Vareda, P. Maximiano, L. P. Cunha, A. F. Ferreira, P. N. Simões, L. Durães, *J Colloid Interf. Sci.* 512 (2018) 64–76.
17. A. Eftekhari, L. Li, Y. Yang, *J. Power Sources*, 347 (2017) 86–107.
18. M. Q. Sun, G. C. Wang, X. W. Li, Q. L. Cheng, C. Z. Li, *Ind. Eng. Chem. Res.*, 51 (2012) 3981−3987.
19. H. P. Cong, X. C. Ren, P. Wang, S. H. Yu, *Energy Environ. Sci.*, 6 (2013) 1185–1191.
20. K. Zhou, Y. He, Q. C. Xu, Q. E. Zhang, A. A. Zhou, Z. H. Lu, L. K. Yang, Y. Jiang, D. T. Ge, X. Y. Liu, H. Bai, *ACS Nano*, 12 (2018) 5888–5894.
21. Z. Q. Tong, Y. N. Yang, J. Y. Wang, J. P. Zhao, B. L. Su, Y. Li, *J. Mater. Chem. A*, 2 (2014) 4642–4651.
22. P. P. Yu, Z. M. Zhang, L. X. Zheng, F. Teng, L. F. Hu, X. S. Fang, *Adv. Energy Mater.*, 6 (2016) 1601111–1601120.
23. F. Huang and D. Chen, *Energy Environ. Sci.*, 5 (2012) 5833–5841.
24. L. J. Ren, G. N. Zhang, Z. Yan, L. Kang, H. Xu, F. Shi, Z. B. Lei, Z. H. Liu, *Electrochim. Acta*, 231 (2017) 705–712.
25. Z. S. Wang, Q. Zhang, S. C. Long, Y. X. Luo, P. K. Yu, Z. B. Tan, J. Bai, B. H. Qu, Y. Yang, J. Shi, H. Zhou, Z. Y. Xiao, W. J. Hong, S. Wang, H. Bai, *ACS Appl. Mater. Interfaces*, 10 (2018) 10437–10444.
26. S. P. Sasikala, K. E. Lee, J. Lim, H. J. Lee, S. H. Koo, I. H. Kim, H. J. Jung, S. O. *ACS Nano*, 11 (2017) 9424–9434.
27. M. M. Mohamed, M. A. Mousa, M. Khairy, A. A. Amer, *ACS Omega*, 3 (2018) 1801–1814.
28. P. C. Du, L. Lin, H. X. Wang, D. Liu, W. L. Wei, J. G. Li, P. Liu, *Mater. Design*, 127 (2017) 76–83.
29. K. Zhang, L. L. Zhang, X. S. Zhao, J. Wu, *Chem. Mater.*, 22 (2010) 1392–1401.
30. C. C. Chang and T. Imae, *ACS Sustainable Chem. Eng.*, 6 (2018) 5162−5172.